Inhibition of lipid metabolism exerts antitumor effects on rhabdomyosarcoma

Satoshi Miyagaki
Department of Pediatrics, Kyoto Prefectural University of Medicine, Graduate School of Medical Science
Ken Kikuchi (ken-k@koto.kpu-m.ac.jp)
Department of Pediatrics, Kyoto Prefectural University of Medicine, Graduate School of Medical Science
Jun Mori
Department of Pediatrics, Kyoto Prefectural University of Medicine, Graduate School of Medical Science
Gary D. Lopaschuk
Department of Pediatrics, Mazankowski Alberta Heart Institute, University of Alberta
Tomoko Iehara
Department of Pediatrics, Kyoto Prefectural University of Medicine, Graduate School of Medical Science
Hajime Hosoi
Department of Pediatrics, Kyoto Prefectural University of Medicine, Graduate School of Medical Science

Research Article

Keywords: Rhabdomyosarcoma (RMS), Warburg effect, vitro , malonyl-CoA decarboxylase

Posted Date: February 1st, 2021

DOI: https://doi.org/10.21203/rs.3.rs-152131/v1

Abstract

Background and aims:

Rhabdomyosarcoma (RMS) exhibits tumor-specific energy metabolic changes that include the Warburg effect. Since targeting cancer metabolism is a promising therapeutic approach, we examined the antitumor effects of suppressing lipid metabolism in RMS.

Methods:

We suppressed lipid metabolism in RMS cells *in vitro* by administering an inhibitor of malonyl-CoA decarboxylase, which increases malonyl CoA and decreases fatty acid oxidation. *In vivo* studies involved injection of human Rh30 cells into the gastrocnemius muscle of 6-week-old female nude mice, which were divided into two groups: normal chow diet group (NCD) and low-fat diet group (LFD).

Results:

Suppression of lipid metabolism in RMS cells decreased cell proliferation by inducing cell cycle arrest. Metabolomic analysis showed an increase in glycolysis and inactivation of the pentose phosphate pathway. Immunoblotting analysis revealed upregulated expression of LC3A/B-II, an autophagy marker, due to increased phosphorylation of AMP-activated protein kinase (AMPK), a nutrient sensor. Inhibition of both lipid metabolism and autophagy suppressed tumor proliferation and increased apoptosis. Moreover, mice fed a LFD for 21-days showed reduced tumor growth compared to NCD-fed mice.

Conclusion:

Suppression of lipid metabolism disrupted the equilibrium of the cancer-specific metabolism in RMS, resulting in a tumor growth-inhibitory effect. Therefore, the development of treatments focusing on the lipid dependence of RMS is highly promising.

Introduction

Rhabdomyosarcoma (RMS), the most prevalent malignancy among pediatric soft tissue tumors [1–3], arises from myogenic mesenchymal progenitors and occurs in various parts and tissues of the body, such as the bladder, gonads, nasopharyngeal cavity, paranasal sinuses, parameninges, orbit, and skeletal muscle [4, 5]. While recent progress in combined modality therapy has slightly improved the prognosis of patients with RMS, long-term organ damage due to treatment-related toxicity has become a serious concern. Therefore, there is an urgent need to develop tumor-specific therapies with few side effects.

Rapidly proliferating cancer cells, especially solid tumor cells, are prone to hypoxia and nutrient starvation, resulting in metabolic reprogramming to maintain their enormous energy demands. It is widely known that glucose uptake is higher in cancer cells than in normal cells. In addition, cancer cells synthesize adenosine triphosphate (ATP) primarily via glycolysis in the cytoplasm, which does not require

oxygen, rather than oxidative phosphorylation in mitochondria, even in an oxygen-rich environment. This phenomenon was first proposed by Otto Warburg approximately 100 years ago, and later named as the Warburg effect or 'aerobic glycolysis' [6, 7]. Moreover, cancer cells activate the pentose phosphate pathway (PPP), a branched pathway from glycolysis, to increase nucleic acid supply in order to maintain their rapid proliferative capacity, and nicotinamide adenine dinucleotide phosphate (NADPH) synthesis to cope with oxidative stress [8, 9]. It has been reported that glycolysis is significantly upregulated in Rh30, an alveolar-type RMS cell line, compared with normal myocytes [10]. Pyruvate kinase M (Pkm) is involved in the synthesis of pyruvate, the final product of glycolysis, and has two splicing variants, Pkm1 and Pkm2 [11]. Pkm1 derived pyruvate is preferentially destined for the mitochondrial tricarboxylic acid (TCA) cycle, while Pkm2 derived pyruvate is predominantly destined for lactate production. Most cancer cells significantly express Pkm2, and Rh30 is no exception [12]. Therefore, glucose taken up by RMS cells is mostly used for lactate synthesis, not glucose oxidation in the mitochondria. However, at the same time, it has been shown that the mitochondrial TCA cycle in Rh30 is enhanced, suggesting that energy substrates other than glucose, such as glutamic acid and fatty acids, may be primarily oxidized [10]. Recently, it has been reported that lipids are indispensable in some types of cancer cells, such as breast and prostate cancer cells. [13, 14]. Both lipid anabolism and catabolism are important metabolic pathways, with lipid anabolism (such as energy storage and lipid synthesis) being essential for cell membrane construction, while lipid catabolism (such as ATP synthesis by fatty acid oxidation) being critical for energy generation.

Thus, we hypothesized that the suppression of lipid metabolism in RMS exerts an antitumor effect through an imbalance in cancer-specific energy metabolism. In the present study, we verified this hypothesis using both *in vitro* and *in vivo* experiments.

Results

Inhibition of lipid metabolism by malonyl-CoA decarboxylase inhibitor (MCDi) suppressed cell proliferation and induced cell cycle arrest in RMS cells.

We investigated the tumor growth inhibitory effect of suppressing lipid metabolism with the MCDi (CBM-3001106) [15, 16]. Administration of the MDCi to the alveolar RMS (ARMS) cell lines Sj-Rh30 (Rh30) and Rh41, and the embryonal RMS (ERMS) cell lines RD and KP-RMS-KH (KH) resulted in concentration- and time-dependent growth inhibitory effects (Fig. 1a). Notably, the mRNA expression level of carnitine palmitoyltransferase (CPT) 1 isozymes, the target of malonyl CoA, were different in each cell line (see Supplementary Fig. S1 online). It has been reported that *PAX3-FKHR* (*PAX3-FOXO1*), a fusion gene characteristic of the ARMS, is involved in the transcription of CPT1A and regulates tumor cell infiltration and metastasis [17]. MCDi administration increases the level of malonyl-CoA, which inhibits CPT1 and reduces fatty acid uptake in mitochondria [18]. In this study, the tumor growth inhibitory effect of MCDi was similar for both the alveolar and embryonal cell lines. Furthermore, the effect of inhibition of lipid metabolism on the cell cycle was examined. Administration of 10 μM MCDi induced G1 cell cycle arrest in

Rh30, Rh41, and RD cell lines with statistically significant differences. In case of KH, there was no significant difference, although a similar trend was observed in which the population of cells in the G1 phase increased ($P = 0.077$) (Fig. 1b).

Metabolomic analysis revealed that lipid metabolism inhibition affects the tumor-specific energy metabolism of RMS cells.

We performed a metabolomic analysis of Rh30 cells treated with dimethylsulfoxide (DMSO) or 10 μM MCDi for 24 h. Reflecting the action of MCDi, a significant increase in malonyl-CoA and decrease in acetyl-CoA levels were observed (Fig. 2a). In addition, the promotion of lactic acid synthesis was confirmed (Fig. 2b). Moreover, a markedly decreased 6-phosphogluconate (6-PG) level, declining NADPH/$NADP^+$ ratio ($P = 0.085$), and significantly increased 6-PG/ribose 5-phosphate (R5P) ratio indicated the inactivation of PPP (Fig. 2c). The levels of intermediate metabolites of the mitochondrial TCA cycle, except for 2-oxoglutaric acid (2-OG), were significantly reduced by the suppression of lipid metabolism (Fig. 2d). Since both glutamine (Gln) and glutamate (Glu) levels were significantly increased by the administration of MCDi (Fig. 2e), it suggests that the increase in 2-OG was a result of the replacement pathway for glutamine degradation. There was no difference in the amount of ATP, although AMP levels were significantly increased in MCDi-treated cells (Fig. 2f). Next, we compared the mRNA expression levels of key enzymes located at the junction of glycolysis to determine whether the changes in these metabolites due to MCDi administration occurred similarly in other RMS cell lines. Lactate dehydrogenase A (LDH-A), an enzyme that converts pyruvate to lactate, did not show a significant change in mRNA expression levels. On the contrary, the expression of pyruvate dehydrogenase (PDH) kinase (PDHK4), which inhibits PDH that converts pyruvate to acetyl-CoA, was significantly increased in all cell lines due to the inhibition of lipid metabolism. In addition, the mRNA expression of glucose 6-phosphate dehydrogenase (G6PD), the first rate-limiting enzyme in the PPP for converting glucose 6-phosphate (G6P) to 6-phosphogluconic acid (6PG), was significantly reduced. These results indirectly demonstrated that the suppression of lipid metabolism by MCDi administration caused similar metabolic changes in all four RMS cell lines (Fig. 2g).

Inhibition of lipid metabolism promoted autophagy signaling via the AMPK-mTOR pathway and increased p21 expression.

Immunoblot analyses were performed to assess the protein expression level of AMP-activated protein kinase (AMPK), which is an important intracellular energy sensor. After the administration of DMSO or 10 μM MCDi for 24 h, the phosphorylation of AMPK was increased (Fig. 3a), as were AMP levels (Fig. 2f), which activates AMPK. Moreover, inhibition of lipid metabolism increased the phosphorylation level of

Tuberous sclerosis 2 (TSC2) located downstream of AMPK. Further, the phosphorylation of p70S6 kinase (p70S6K), located downstream of mammalian target of rapamycin complex 1 (mTORC1), was reduced. Protein expression of p21, a cell cycle suppressor, was also increased. Moreover, LC3A/B-II protein levels were increased after MCDi administration (Fig. 3a). Usually, when autophagy is promoted, LC3-I is converted into its phosphatidylethanolamine-conjugated form, LC3-II, which is a key factor in the maturation of autophagosome. Immunofluorescence staining revealed that the inhibition of lipid metabolism increased the level of LC3 puncta in the cytoplasm of RMS cells, indicating the formation of autophagosomes (Fig. 3b).

Inhibiting both lipid metabolism and autophagy suppressed tumor cell proliferation with increased apoptotic cell death.

Based on the above results, we investigated whether the autophagy induced by the inhibition of lipid metabolism was a tumor-protective response or the cytotoxic event known as autophagic cell death. Bafilomycin A1 (BafA1) inhibits late phase autophagy by preventing the maturation of autophagic vacuoles through the inhibition of fusion between autophagosomes and lysosomes. When MCDi and BafA1 were used together, cell proliferation was suppressed to a greater degree in the combination group than in the single-agent groups (Fig. 4a). Apoptosis analysis revealed that the annexin V-positive cell population increased following concomitant administration, suggesting further induction of apoptotic cell death (Fig. 4b and 4c).

A fat-restricted diet suppressed RMS growth in the orthotopic xenograft mouse model through decreasing lipid metabolism.

After confirming the engraftment of transplanted luciferase-positive Rh30 cells in a xenograft mouse model, the bioluminescence of the tumor cells was evaluated over a 3- week period after starting the NCD or the LFD. LFD-fed mice had lower tumor-related bioluminescence intensities than NCD-fed mice (Fig. 5a). At 21 days after diet change, the tumor sizes of LFD-fed mice were smaller than those of NCD-fed mice (Fig. 5b). During the observation period, there was no significant difference in body weight and calorie intake between the NCD and LFD fed mice (Fig. 5c and 5d). Next, we euthanized the mice to excise the tumor mass and performed immunohistochemical staining with an anti-Ki67 antibody. The Ki67-positive rate was significantly lower in tumor samples from LFD-fed mice than in those from NCD-fed mice (Fig. 5e). Moreover, the mRNA expression levels of CPT1 isozymes, which are rate-limiting enzymes for lipid metabolism in mitochondria, were compared using the tumor samples. In tumors of LFD-fed mice, the expression level of CPT1A mRNA was significantly lower than that in tumors of NCD-fed mice, and CPT1B tended to decrease (Fig. 5f). In addition, G6PD mRNA expression was relatively reduced in LFD-fed mice than in the NCD-fed mice ($P = 0.076$) (Fig. 5g).

Discussion

Therapeutic approaches that specifically target tumors and have few systemic side effects are important for cancer treatment. In recent years, many researchers have focused on therapeutic strategies targeting tumor-specific energy metabolism. However, there are few studies on cancer metabolism in childhood cancers, especially RMS. The present study yields novel findings concerning a therapeutic strategy for RMS, focusing on lipid metabolism.

It has been previously reported that the Warburg effect exists in RMS [10, 12]. The verification of intracellular metabolism using stable isotopes revealed that glucose uptake was significantly increased and lactate synthesis was enhanced in Rh30 compared to normal myocytes, demonstrating upregulated glycolytic function in RMS [10]. Moreover, the mitochondrial TCA cycle was upregulated in Rh30 [10], indicating that energy substrates other than glucose, such as glutamic acid and fatty acids, were also essential for the TCA cycle. Thus, we hypothesized that suppressing lipid metabolism in RMS would upset the balance of tumor-specific energy metabolism, or the Warburg effect, leading to an antitumor effect.

Metabolomic analysis revealed that most intermediates in the mitochondrial TCA cycle were significantly reduced by the administration of MCDi, as would be expected if fatty acid oxidation was inhibited. Only 2-OG among the intermediate metabolites of the TCA cycle showed increased levels, likely owing to the anaplerotic pathway, which takes up glutamate from the cytoplasm into the mitochondria, [19]. The metabolomic analysis further revealed that the PPP was down-regulated and nucleic acid synthesis was suppressed in RMS treated with the MCDi. AMPK is a key nutrient sensor that controls various intracellular signals by reflecting the nutritional status, not only in normal cells but also in tumor cells [20]. Recently, AMPK has been reported to suppress the expression of G6PD, the rate-limiting enzyme in the first stage of PPP, by inactivating the transcriptional activities of cyclic AMP-response element-binding protein (CREB) and CREB-regulated transcriptional coactivator-1 (CRTC-1) [21, 22]. In our study, the inhibition of lipid metabolism in RMS cell lines increased AMPK phosphorylation, reflecting the intracellular low-energy state, and suppressed the expression of G6PD mRNA. This suggests that the inhibition of lipid metabolism suppressed the PPP in RMS cells via the AMPK-CRCT1-CREB-G6PD pathway. The inhibition of lipid metabolism induced cell cycle arrest in the G1 phase and increased the expression of p21 protein in all RMS cell lines. p21 is a major target of p53 activity and is thus associated with cell cycle arrest. In RMS cells, especially Rh30, Rh41, and RD cell lines, the tumor suppressor protein p53 is either mutated or deleted, and therefore its function is suppressed [23–25]. The inhibition of lipid metabolism suppressed the PPP in RMS cells, which might induce G1 arrest by promoting p21 expression via a p53-independent pathway [26, 27]. Overall, we proposed that the imbalanced tumor-specific energy metabolism due to the suppression of lipid metabolism led to an antitumor effect against RMS cells.

Autophagy facilitates the production of energy substrates required for cells to maintain their survival during starvation and breaks down the waste products accumulated inside cells, such as abnormal proteins and organelles with reduced function [28, 29]. While various signals control autophagy, AMPK is

a major factor that induces autophagy, especially under nutrient deprivation [30]. mTORC1 is a major suppressor of autophagy signals [31]. As mentioned above, AMPK inhibits mTORC1 through the activation of TSC2 and also directly activates the unc-51 like autophagy activating kinase (Ulk1), followed by the induction of autophagy signals [32, 33]. Autophagy is present not only in normal cells but also in cancer cells [29, 34]. In this study, the suppression of lipid metabolism increased AMPK phosphorylation in RMS cell lines, resulting in the activation of the autophagy pathway. Additionally, western blotting and immunofluorescence staining confirmed the increased expression of LC3-II protein, which is a component of the autophagosome membrane and is therefore considered to be an autophagy marker.

Previous studies have shown that the role of autophagy, whether beneficial or harmful to tumors, is complex depending on the type of cancer. The advantage of autophagy in cancer cells is its protective role against various environmental stressors, and blocking this compensatory response increases cancer cell death [35, 36]. On the contrary, the activation of the autophagy pathway itself induces cancer cell death, which is called autophagic cell death [37]. This type of programmed cell death is defined by the reduction of cancer cell death due to inhibition of autophagy. It has been reported that several therapeutic approaches induced autophagy in RMS. In addition, when the increased autophagy was suppressed, the apoptotic cell death was induced. [38, 39]. Consistent with these previous studies, we found that the suppression of lipid metabolism in RMS induced autophagy. Moreover, the inhibition of autophagy led to the promotion of apoptosis. Therefore, autophagy plays a tumor-protective role in RMS, and combination therapy by suppressing both lipid metabolism and autophagy may be promising as a therapeutic strategy.

Based on the results of *in vitro* experiments, we examined the lipid-dependence of RMS in orthotopic xenograft models by restricting dietary exogenous fats. Comparison between NCD-fed and LFD-fed mice showed no significant difference in body weight and total calorie intake during the observation period. However, bioluminescence imaging showed significantly suppressed tumor growth in LFD-fed mice compared to that in NCD-fed mice. Since calorie restriction was not involved, the difference in exogenous lipid uptake between the two groups was considered to be the cause of this difference. Moreover, CPT1A mRNA expression was significantly decreased in the tumors of LFD-fed mice, suggesting that not only the uptake of exogenous lipids but also the import of fatty acids into mitochondria were reduced. A significant decrease in the expression level of Ki67, a cell cycle-related protein, was observed in LFD-fed mice, indicating that the reduced lipid metabolism led to the suppression of the cell cycle. PPP might also have been affected, as the expression of G6PD mRNA tended to decrease. Thus, our *in vivo* experiments showed that the reduced exogenous lipid supply due to LFD affected lipid metabolism in RMS and exerted a tumor growth inhibitory effect.

Recently, there have been reports that HFD promotes the growth of several types of tumors. In colorectal cancer, increased level of HFD-derived palmitic acid induced the activation of hormone-sensitive lipase through the upregulation of cAMP/PKA signaling, which was promoted by increasing β2 adrenergic receptor expression, and enhancing the supply of fatty acids as an energy substrate in tumor cells; this

affected the metabolic phenotype and made the tumor more malignant [40]. HFD also increases the population of myeloid-derived suppressor cells, which have been reported as facilitators of tumor growth, resulting in the stimulation of inflammation in the microenvironment surrounding cancer cells and affecting the malignancy of the tumor [41, 42]. In other words, the availability of a large amount of fatty acids contributes to tumor growth in various ways. Like normal cells, cancer cells have lipid droplets in their cytoplasm, which enable them to adjust to adverse conditions such as starvation and oxidative stress [43]. Furthermore, many lipid metabolism-related enzymes are associated with the undesirable characteristics of cancer cells, such as invasion and metastasis [44]. High lipid availability is advantageous for tumor cells, whereas low lipid content may be disadvantageous for cancer growth; however, there have been few reports indicating that the suppression of lipid utilization exerts an antitumor effect.

The limitations of the present study are below: In the *in vitro* experiments, we only compared the effects of using the drug that suppresses intracellular lipid metabolism, and did not compare the effects on inhibiting the utilization of the exogeneous lipids, such as by reducing the fat content in the medium. Moreover, the biological experiments in this study were conducted in mice, and the effects of lipid metabolism inhibition on humans need to be fully investigated in the future.

In conclusion, the present study revealed that the inhibition of lipid metabolism suppressed the PPP in RMS. As a result, the synthesis of nucleic acids essential for the growth of cancer cells and antioxidants required for maintaining oxidative balance decreased, leading to a tumor growth inhibitory effect due to cell cycle arrest. It has been suggested that AMPK might play a key role in this antitumor effect. The autophagy signals induced by the AMPK-mTOR pathway were thought to be a tumor-protective reaction in RMS. This is because apoptotic cell death was induced via inhibition of the autophagy which was promoted by suppressing of the lipid metabolism. Including the experimental results in cancer-bearing mouse models, we reported for the first time that RMS relies on lipid metabolism to maintain its growth. Therefore, we believe that reducing lipid intake is a promising therapeutic approach for the treatment of RMS.

Materials And Methods

Cell culture

We used the following human alveolar RMS (ARMS) cell lines: SJ-Rh30 (Rh30) and Rh41 that were kindly provided by Peter J. Houghton, M.D (the Greehey Children's Cancer Research Institute, University of Texas Health Science Center, San Antonio TX, USA) and human embryonal RMS (ERMS) cell lines, RD was obtained from JCRB (Japanese Collection of Research Bioresources) Cell Bank, and KP-RMS-KH (KH) [45]. Cells were cultured in Dulbecco's modified Eagle's medium (DMEM) supplemented with 1% fetal bovine serum (FBS) and 1% penicillin-streptomycin at 37°C in a 5% CO_2 incubator; 1% FBS was used to imitate the living environment typical of various solid tumors, where nutrients and growth factors are likely to be deficient due to the inadequate vascularization.

Animals and Diets

For this study, 5-week-old female BALB/c nu/nu nude mice (n = 10, bodyweight 16–18 g) were purchased from Japan SLC, Inc. (Japan). All experiments and procedures were conducted in accordance with the Institutional Animal Care and Use Committee guidelines. Animal experiments were approved by the Committee for Animal Research of Kyoto Prefectural University of Medicine (Authorization No. M2019-516). We injected 5×10^6 luciferase-positive Rh30 cells into the right gastrocnemius muscle of the mice (orthotropic xenograft model). After confirming tumor engraftment, the mice were randomly divided into two groups: one group was fed a normal chow diet (NCD; fat content 12.0%/kcal) and the other group was fed a low-fat diet (LFD; fat content 1.3%/kcal). These diets were prepared by CLAIR Japan Inc. Animals received food and sterile water *ad libitum*. Food intake was measured during the experiments. Tumor growth was monitored using *in vivo* bioluminescence images twice a week. The mice were intraperitoneally injected with D-luciferin (150 mg/kg) 10 min before imaging and then anesthetized with 2% isoflurane during imaging in the chamber. IVIS Lumina Series III (PerkinElmer, Inc., USA) detected the photons from the mice, and Living Image v.2 (PerkinElmer, Inc., USA) quantified regions of interest (ROIs) on the displayed images in photons per second (ph/s). These animal experiments were performed in accordance with the Animal Research Reporting *In Vivo* experiments (ARRIVE) guidelines.

Inhibitory reagents

MCDi was kindly provided by Gary D. Lopaschuk. MCDi inhibits the conversion of malonyl-CoA to acetyl-CoA by malonyl-CoA decarboxylase, resulting in an increase in malonyl-CoA level in the cytoplasm. Increased malonyl-CoA suppresses fatty acid uptake through CPT1, which is a rate-limiting enzyme of fatty acid β-oxidation in the mitochondrial outer membrane [15, 16]. Baf A1 was purchased from Cayman Chemical (Ann Arbor, MI, USA). These reagents were dissolved in dimethyl sulfoxide (DMSO) at the concentration used. In all experiments, the percentage of DMSO was less than 0.01%.

WST-8 cell viability assay

To assess cell viability, we performed WST-8 colorimetric assays using Cell Counting Kit-8 (Nacalai Tesque, Kyoto, Japan) according to the manufacturer's protocol. The cells described above were seeded in 96-well plates in 100 μl culture medium for 24 h and the necessary reagents were added. Cell viability was determined by measuring the optical density (OD) at 450 nm with a microplate reader (Multiskan™ JX; Thermo Labsystems, Santa Rosa, CA, USA).

Cell cycle analysis

To examine the effects of MCDi on the cell cycle, we cultured RMS cell lines with 0 or 10 μM MCDi for 24 h. The cells were then isolated by scraping, washed with phosphate-buffered saline (PBS), and incubated at room temperature (20–25 °C) with propidium iodide for 30 min to stain the DNA. We determined the DNA content using a FACS Calibur flow cytometer (BD Bioscience) and analyzed the status of the cell cycle using FlowJo v.9 (FlowJo LLC, USA), as described previously [1].

Apoptosis analysis

We analyzed cell death after Annexin V-FITC / propidium iodide staining using a TACS annexin-V apoptosis detection kit (R&D System, USA) according to the manufacturer's instructions. We analyzed the data using FlowJo.

Quantitative real-time PCR

To determine the mRNA expression levels, we extracted total RNA from RMS cell lines and tumor tissues removed from xenograft models using a NucleoSpin RNA II kit (Macherey-Nagel, Duren, Germany). cDNA was synthesized using ReverTra Ace qPCR RT Master Mix (Toyobo, Osaka, Japan). We prepared the working solution for quantitative real-time PCR (qRT-PCR) with TB Green Premix Ex Taq II (Tli RNaseH Plus) (Takara, Shiga, Japan) and analyzed it using the AB 7500 Real-Time PCR System (Applied Biosystems, Tokyo, Japan). The PCR steps were as follows: initial denaturation at 95°C for 30 s, followed by 40 cycles of 95°C for 5 s, and 60°C for 34 s. The PCR primer sequences are shown in Supplementary Table S1 online. β-actin was used as the internal standard.

Western blot

RMS cell lines were administered with MCDi or DMSO control and incubated for 24 h. Cells were then lysed with radioimmunoprecipitation assay (RIPA) lysis buffer (Nacalai Tesque, Kyoto, Japan). The products obtained by homogenization were centrifuged at 10,000×g for 5 min at 4°C and the supernatants were collected. We measured protein concentrations by using a Bio-Rad protein assay kit (Bio-Rad, Tokyo, Japan). The proteins were electrophoresed on 4–20% sodium dodecyl sulfate polyacrylamide gels, as followed by transferring onto polyvinylidene difluoride (PVDF) membranes and blocking with Blocking One (Nacalai Tesque). Can Get Signal Solution 1 and 2 (Toyobo, Osaka, Japan) were used to diluted the primary and secondary antibodies, respectively. The membrane was incubated with primary antibodies against total AMP-activated protein kinase (1:1,000) (AMPKα; Cell Signaling Technology (CST)), phospho-AMPKα (1:1,000) (Thr172; CST), tuberous sclerosis 2 (1:1,000) (TSC2; CST), phospho-TSC2 (1:1,000) (CST), p70S6kinase (1:1,000) (p70S6K, CST), phospho-p70S6K (1:1,000) (CST), Waf-p21 (1:1,000) (p21; CST), LC3A/B (1:1,000) (CST), and β-actin (1:5,000) (CST). The secondary antibody was dissolved with horseradish peroxidase (HRP)-conjugated donkey anti-rabbit immunoglobulin G (IgG) to a concentration of 1:10,000 (for AMPK, p-AMPK, TSC2, p-TSC2, p70S6K, p-p70S6K, p21, LC3A/B) (GE Healthcare, Tokyo, Japan) or HRP-conjugated sheep anti-mouse IgG (for β-actin) (GE Healthcare). Antibody binding was identified using an enhanced HRP-luminol chemiluminescence system. The raw data of western blotting is represented in Supplementary Figure S2 online.

Immunofluorescence microscopy

The cells were cultured on Falcon 8-well Culture Slides (354118, BD Falcon, Corning, Inc., Corning, NY, USA), then fixed with 4% paraformaldehyde for 20 min at room temperature, permeabilized with 0.1% Triton X-100, washed with PBS, and blocked with Blocking One Histo (Nacalai Tesque, Kyoto, Japan). Then, they were incubated with anti-LC3A/B antibody (1:100, Cell Signaling Technology) overnight at 4°C, and goat anti-rabbit IgG (H + L) cross-absorbed secondary antibody, Alexa Flour 488 (A-11008, 1:200, Life

Technologies, Tokyo, Japan) for 2 h at room temperature (20–25°C) with shading. Nuclei were stained with HardSet Antifade Mounting Medium with DAPI (H-1500, Vector Laboratories, CA, USA) for 15 min. Finally, we observed the slides using a fluorescence microscope system, KEYENCE BZ-X710 instrument (Keyence Corp., Osaka, Japan).

Immunohistochemistry

Immunohistochemical staining was performed as described previously [46]. Briefly, tumors removed from the xenografted mice were fixed with 4% paraformaldehyde and the fixed tissues were embedded in paraffin, sliced to a thickness of 4 μm, and placed on glass slides. After deparaffinization and rehydration, tissue antigens were retrieved with citrate buffer (pH 6), and endogenous peroxidase activity was inhibited by incubating the tissue sections with 3% H_2O_2 for 10 min. The sections were then blocked with blocking solution (Blocking One Histo, Nacalai Tesque) and incubated with mouse anti-Ki67 antibody (M7240, dilution 1:100, DAKO, Glostrup, Denmark) for 20 min at room temperature. Incubation with the secondary antibody (HRP-conjugated goat anti-mouse IgG antibody; ab214879, pre-diluted, Abcam) was performed at room temperature for 30 min. Hematoxylin (8656, Sakura Finetek, Japan) was used for counterstaining the nucleus. The signals were detected by DAB (K3468, DAKO).

Metabolomics analysis

We performed metabolomic analysis using C-Scope (Human Metabolome Technologies, Yamagata, Japan), according to the recommended protocol [47]. Rh30 cells administered with DMSO or MCDi (10 μM) for 24 h were used as samples. In brief, after washing twice with 5% mannitol solution, 800 μl methanol and 550 μl of 8 μM internal standard were added to the cells. Next, the cells were centrifuged at 4°C, 2,300 x *g* for 5 min. The supernatants were then collected by centrifugation through a 5 kDa-cutoff filter at 4°C, 8,100 x *g* for 3 h. The concentrations of all charged compounds were measured by capillary electrophoresis time-of-flight mass spectrometry (CE-TOFMS) and capillary electrophoresis tandem mass spectrometry (CE-QqQMS; CE-MS/MS) according to a previously described method [48].

Statistical analysis

All data are presented as the mean ± standard deviation (SD). To compare the means between groups, we used a two-tailed *t*-test in Figs. 1, 2, and 4 (n = 3 or 4). Mann-Whitney's U-test was performed for the analysis in Fig. 5 (n = 5 in each group). Differences with a *P*-value < 0.05 were considered statistically significant.

Declarations

Acknowledgements

We thank Peter J. Houghton, M.D. of the Greehey Children's Cancer Research Institute, University of Texas Health Science Center, San Antonio, TX, USA, for providing the cell lines Rh30 and Rh41. We are grateful

to Yasuhiro Kawabe and Youhei Sugimoto for teaching experimental techniques. We would like to thank Editage (www.editage.com) for English language editing.

Funding

This work was supported by the grant received from Children's Cancer Association of Japan.

Author contributions

S.M., K.K., J.M. and H.H. conceived and designed this study. Experimental methodology was developed by K.K.. Experimental procedures were carried out by S.M.. G.D.L. developed MCDi (CBM-3001106). All authors participated in the analysis and interpretation of data. S.M., J.M., K.K. performed the statistical analysis and wrote the manuscript. All authors read and approved the manuscript and agree to be accountable for all aspects of the research in ensuring that the accuracy or integrity of any part of the work are appropriately investigated and resolved.

Competing interests

The authors declare no competing interests.

References

1. Kikuchi, K. *et al.* Cell-cycle dependent expression of a translocation-mediated fusion oncogene mediates checkpoint adaptation in rhabdomyosarcoma. *PLOS Genet.* **10**(1), e1004107 (2014). 1371/journal.pgen.1004107, Pubmed:24453992.
2. Otabe, O. *et al.* MET/ERK2 pathway regulates the motility of human alveolar rhabdomyosarcoma cells. *Rep.* **37**(1), 98-104 (2017). 10.3892/or.2016.5213, Pubmed:27840956.
3. Hayes-Jordan, A. & Andrassy, R. Rhabdomyosarcoma in children. *Opin. Pediatr.* **21**(3), 373-378 (2009). 10.1097/MOP.0b013e32832b4171, Pubmed:19448544.
4. Xia, S. J., Pressey, J. G. & Barr, F. G. Molecular pathogenesis of rhabdomyosarcoma. *Cancer Biol. Ther.* **1**(2), 97-104 (2002). 4161/cbt.51, Pubmed:12170781.
5. Panda, S. P. *et al.* Diagnosis and management of rhabdomyosarcoma in children and adolescents: ICMR consensus document. *Indian J. Pediatr.* **84**(5), 393-402 (2017). 1007/s12098-017-2315-3, Pubmed:28378141.
6. Warburg, O. On the origin of cancer cells. *Science* **123**(3191), 309-314 (1956). 1126/science.123.3191.309, Pubmed:13298683.
7. De Preter, G. *et al.* Inhibition of the pentose phosphate pathway by dichloroacetate unravels a missing link between aerobic glycolysis and cancer cell proliferation. *Oncotarget* **7**(3), 2910-2920

(2016). 18632/oncotarget.6272, Pubmed:26543237.

8. Patra, K. C. & Hay, N. The pentose phosphate pathway and cancer. *Trends Biochem. Sci.* **39**(8), 347-354 (2014). 1016/j.tibs.2014.06.005, Pubmed:25037503.
9. Jiang, P., Du, W. & Wu, M. Regulation of the pentose phosphate pathway in cancer. *Protein Cell* **5**(8), 592-602 (2014). 1007/s13238-014-0082-8, Pubmed:25015087.
10. Fan, T. W. *et al.* Rhabdomyosarcoma cells show an energy producing anabolic metabolic phenotype compared with primary myocytes. *Cancer* **7**, 79 (2008). 10.1186/1476-4598-7-79, Pubmed:18939998.
11. Noguchi, T., Inoue, H. & Tanaka, T. The M1- and M2-type isozymes of rat pyruvate kinase are produced from the same gene by alternative RNA splicing. *Biol. Chem.* **261**(29), 13807-13812 (1986). Pubmed:3020052.
12. Sugito, N. *et al.* Cancer-specific energy metabolism in rhabdomyosarcoma cells is regulated by microRNA. *Nucleic Acid Ther.* **27**(6), 365-377 (2017). 1089/nat.2017.0673, Pubmed:28981396.
13. Deberardinis, R. J., Sayed, N., Ditsworth, D. & Thompson, C. B. Brick by brick: metabolism and tumor cell growth. *Opin. Genet. Dev.* **18**(1), 54-61 (2008). 10.1016/j.gde.2008.02.003, Pubmed:18387799.
14. Menendez, J. A. Fine-tuning the lipogenic/lipolytic balance to optimize the metabolic requirements of cancer cell growth: molecular mechanisms and therapeutic perspectives. *Biophys. Acta* **1801**(3), 381-391 (2010). 10.1016/j.bbalip.2009.09.005, Pubmed:19782152.
15. Samokhvalov, V. *et al.* Inhibition of malonyl-CoA decarboxylase reduces the inflammatory response associated with insulin resistance. *J. Physiol. Endocrinol. Metab.* **303**(12), E1459-E1468 (2012). 10.1152/ajpendo.00018.2012, Pubmed:23074239.
16. Ussher, J. R. *et al.* Genetic and pharmacological inhibition of malonyl CoA decarboxylase does not exacerbate age-related insulin resistance in mice. *Diabetes* **65**(7), 1883-1891 (2016). 2337/db15-1145, Pubmed:27207536.
17. Liu, L., Wang, Y. D., Wu, J., Cui, J. & Chen, T. Carnitine palmitoyltransferase 1A (CPT1A): a transcriptional target of PAX3-FKHR and mediates PAX3-FKHR-dependent motility in alveolar rhabdomyosarcoma cells. *BMC Cancer* **12**, 154 (2012). 1186/1471-2407-12-154, Pubmed:22533991.
18. Fillmore, N. & Lopaschuk, G. D. Malonyl CoA: A promising target for the treatment of cardiac disease. *IUBMB Life* **66**(3), 139-146 (2014). 1002/iub.1253, Pubmed:24591219.
19. DeBerardinis, R. J. *et al.* Beyond aerobic glycolysis: transformed cells can engage in glutamine metabolism that exceeds the requirement for protein and nucleotide synthesis. *Natl Acad. Sci. U. S. A.* **104**(49), 19345-19350 (2007). 10.1073/pnas.0709747104, Pubmed:18032601.
20. Shaw, R. J. *et al.* The tumor suppressor LKB1 kinase directly activates AMP-activated kinase and regulates apoptosis in response to energy stress. *Natl Acad. Sci. U. S. A.* **101**(10), 3329-3335 (2004). 10.1073/pnas.0308061100, Pubmed:14985505.
21. Mair, W. *et al.* Lifespan extension induced by AMPK and calcineurin is mediated by CRTC-1 and CREB. *Nature* **470**(7334), 404-408 (2011). 1038/nature09706, Pubmed:21331044.

22. Laliotis, G. P., Bizelis, I., Argyrokastritis, A. & Rogdakis, E. Cloning, characterization and computational analysis of the 5' regulatory region of ovine glucose 6-phosphate dehydrogenase gene. *Biochem. Physiol. B Biochem. Mol. Biol.* **147**(4), 627-634 (2007). 10.1016/j.cbpb.2007.04.001, Pubmed:17493856.

23. Hinson, A. R. *et al.* Human rhabdomyosarcoma cell lines for rhabdomyosarcoma research: utility and pitfalls. *Oncol.* **3**, 183 (2013). 10.3389/fonc.2013.00183, Pubmed:23882450.

24. Miyachi, M. *et al.* Restoration of p53 pathway by nutlin-3 induces cell cycle arrest and apoptosis in human rhabdomyosarcoma cells. *Cancer Res.* **15**(12), 4077-4084 (2009). 10.1158/1078-0432.CCR-08-2955, Pubmed:19509161

25. Shern, J. F. *et al.* Comprehensive genomic analysis of rhabdomyosarcoma reveals a landscape of alterations affecting a common genetic axis in fusion-positive and fusion-negative tumors. *Cancer Discov.* **4**(2), 216-231 (2014). 1158/2159-8290.CD-13-0639, Pubmed:24436047.

26. Mahyar-Roemer, M. & Roemer, K. p21 Waf1/Cip1 can protect human colon carcinoma cells against p53-dependent and p53-independent apoptosis induced by natural chemopreventive and therapeutic agents. *Oncogene* **20**(26), 3387-3398 (2001). 1038/sj.onc.1204440, Pubmed:11423989.

27. Tinkum, K. L. *et al.* Forkhead box O1 (FOXO1) protein, but not p53, contributes to robust induction of p21 expression in fasted mice. *Biol. Chem.* **288**(39), 27999-28008 (2013). 10.1074/jbc.M113.494328, Pubmed:23918930.

28. Mizushima, N., Yoshimori, T. & Ohsumi, Y. The role of Atg proteins in autophagosome formation. *Rev. Cell Dev. Biol.* **27**, 107-132 (2011). 10.1146/annurev-cellbio-092910-154005, Pubmed:21801009.

29. Kimmelman, A. C. & White, E. Autophagy and tumor metabolism. *Cell Metab.* **25**(5), 1037-1043 (2017). 1016/j.cmet.2017.04.004, Pubmed:28467923.

30. Kim, J., Kundu, M., Viollet, B. & Guan, K. L. AMPK and mTOR regulate autophagy through direct phosphorylation of Ulk1. *Cell Biol.* **13**(2), 132-141 (2011). 10.1038/ncb2152, Pubmed:21258367.

31. Thoreen, C. C. *et al.* An ATP-competitive mammalian target of rapamycin inhibitor reveals rapamycin-resistant functions of mTORC1. *Biol. Chem.* **284**(12), 8023-8032 (2009). 10.1074/jbc.M900301200, Pubmed:19150980.

32. Mao, K. & Klionsky, D. J. AMPK activates autophagy by phosphorylating ULK1. *Res.* **108**(7), 787-788 (2011). 10.1161/RES.0b013e3182194c29, Pubmed:21454792.

33. Mack, H. I., Zheng, B., Asara, J. M. & Thomas, S. M. AMPK-dependent phosphorylation of ULK1 regulates ATG9 localization. *Autophagy* **8**(8), 1197-1214 (2012). 4161/auto.20586, Pubmed:22932492.

34. Amaravadi, R., Kimmelman, A. C. & White, E. Recent insights into the function of autophagy in cancer. *Genes Dev.* **30**(17), 1913-1930 (2016). 1101/gad.287524.116, Pubmed:27664235.

35. Feng, H. *et al.* Apatinib-induced protective autophagy and apoptosis through the AKT-mTOR pathway in anaplastic thyroid cancer. *Cell Death Dis.* **9**(10), 1030 (2018). 1038/s41419-018-1054-3, Pubmed:30301881.

36. Ma, R. *et al.* Inhibition of autophagy enhances the antitumour activity of tigecycline in multiple myeloma. *Cell. Mol. Med.* **22**(12), 5955-5963 (2018). 10.1111/jcmm.13865, Pubmed:30247801.
37. Yao, Z. Q. *et al.* A novel small-molecule activator of Sirtuin-1 induces autophagic cell death/mitophagy as a potential therapeutic strategy in glioblastoma. *Cell Death Dis.* **9**(7), 767 (2018). 1038/s41419-018-0799-z, Pubmed:29991742.
38. Moghadam, A. R. *et al.* Autophagy modulates temozolomide-induced cell death in alveolar rhabdomyosarcoma cells. *Cell Death Discov.* **4**, 52 (2018). 1038/s41420-018-0115-9, Pubmed:30416757.
39. Wang, C. *et al.* PFK15, a PFKFB3 antagonist, inhibits autophagy and proliferation in rhabdomyosarcoma cells. *J. Mol. Med.* **42**(1), 359-367 (2018). 10.3892/ijmm.2018.3599, Pubmed:29620138.
40. Fatima, S. *et al.* High-fat diet feeding and palmitic acid increase CRC growth in beta2AR-dependent manner. *Cell Death Dis.* **10**(10), 711 (2019). 1038/s41419-019-1958-6, Pubmed:31558710.
41. Hayashi, T. *et al.* High-fat diet-induced inflammation accelerates prostate cancer growth via IL6 signaling. *Cancer Res.* **24**(17), 4309-4318 (2018). 10.1158/1078-0432.CCR-18-0106, Pubmed:29776955.
42. Clements, V. K. *et al.* Frontline Science: high fat diet and leptin promote tumor progression by inducing myeloid-derived suppressor cells. *Leukoc. Biol.* **103**(3), 395-407 (2018). 10.1002/JLB.4HI0517-210R, Pubmed:29345342.
43. Petan, T., Jarc, E. & Jusović, M. Lipid droplets in cancer: guardians of fat in a stressful world. *Molecules* **23**(8) (2018). 3390/molecules23081941, Pubmed:30081476.
44. Luo, X. *et al.* Emerging roles of lipid metabolism in cancer metastasis. *Cancer* **16**(1), 76 (2017). 10.1186/s12943-017-0646-3, Pubmed:28399876.
45. Nakagawa, N. *et al.* Mutation in the RAS pathway as potential precision medicine targets in treatment of rhabdomyosarcoma. *Biochem Biophys Res Commun.* **512**(3), 524-530 (2019). 1016/j.bbrc.2019.03.038, PubMed:30904164.
46. Cao, D. *et al.* A new tumorsphere culture condition restores potentials of self-renewal and metastasis of primary neuroblastoma in a mouse neuroblastoma model. *PLOS ONE* **9**(1), e86813 (2014). 1371/journal.pone.0086813, Pubmed:24466252.
47. Makinoshima, H. *et al.* Epidermal growth factor receptor (EGFR) signaling regulates global metabolic pathways in EGFR-mutated lung adenocarcinoma. *Biol. Chem.* **289**(30), 20813-20823 (2014). 10.1074/jbc.M114.575464, Pubmed:24928511.
48. Soga, T. *et al.* Differential metabolomics reveals ophthalmic acid as an oxidative stress biomarker indicating hepatic glutathione consumption. *Biol. Chem.* **281**(24), 16768-16776 (2006). 10.1074/jbc.M601876200, Pubmed: 16608839.

Figures

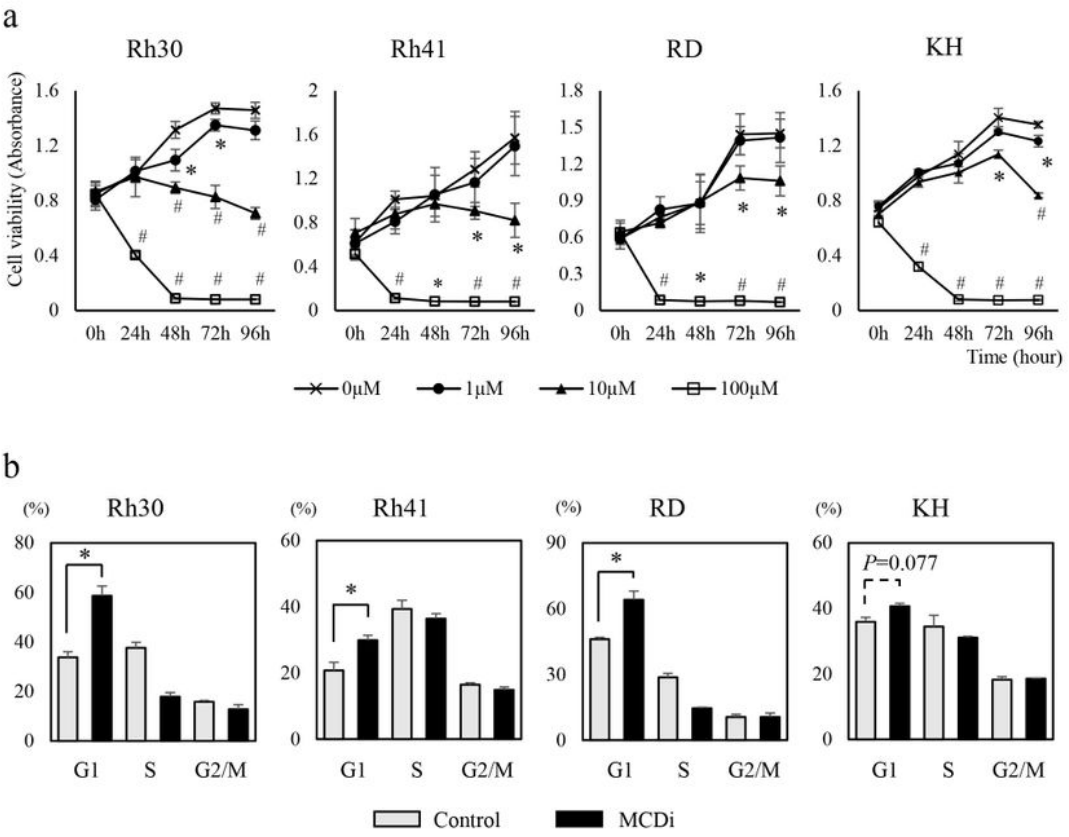

Figure 1. Miyagaki S, *et al.*

Figure 1

The inhibition of lipid metabolism in RMS cell lines induced the suppression of cell proliferation and cell cycle arrest. (a) WST8 assay was performed to create the growth curve over 96 h after the administration of MCDi. (b) Cell cycle assay was analyzed by flow cytometry to calculate the percentage of cells present in each phase of the cell cycle at 24 h after drug administration (Control (DMSO) vs. MCDi 10 μM). All

results are shown as mean ± SD of three independent experiments. (*, P < 0.05 vs. control; #, P < 0.01 vs. control.)

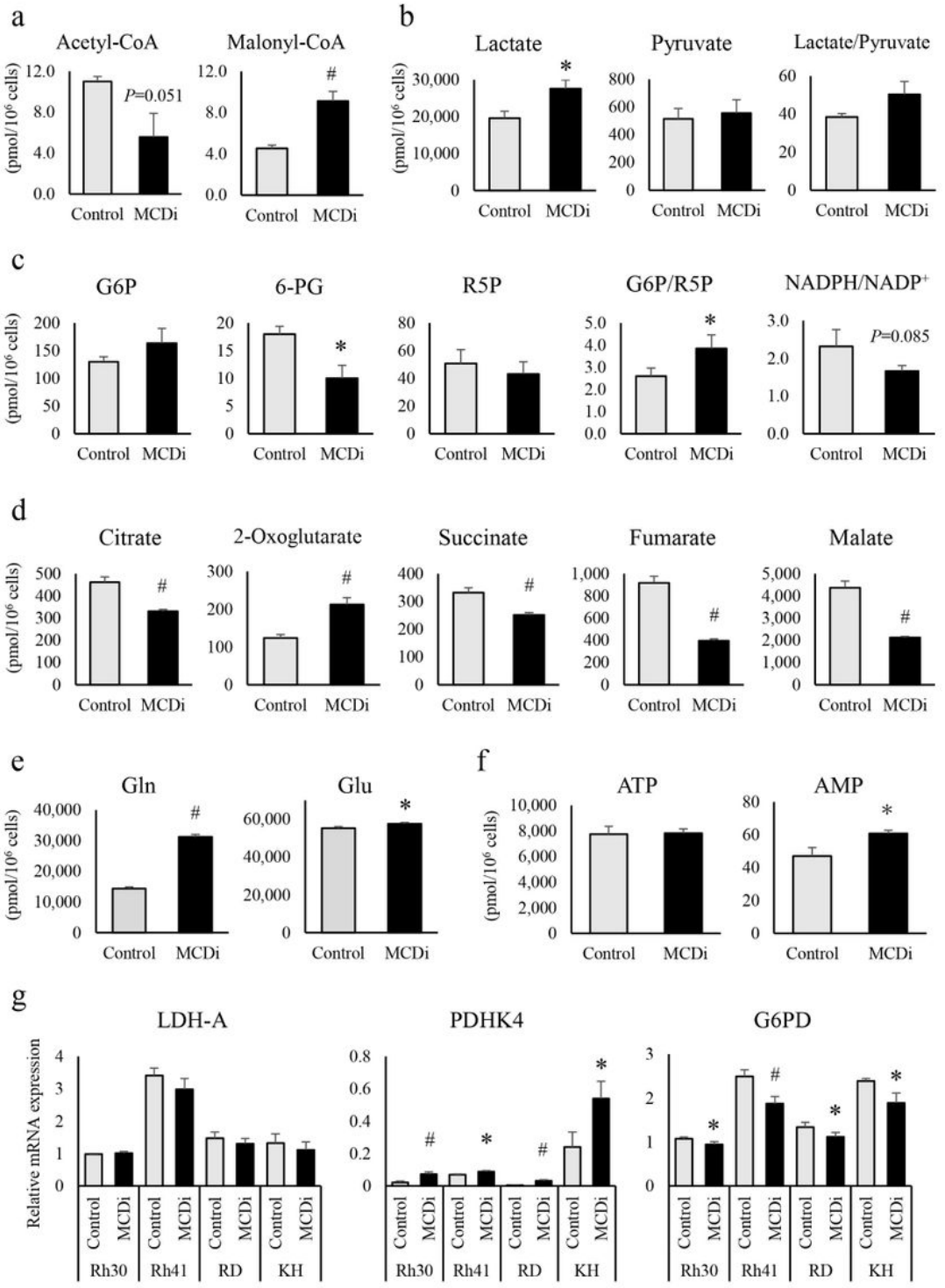

Figure 2. Miyagaki S, *et al.*

Figure 2

a-f; Metabolomic analysis confirmed that the inhibition of lipid metabolism altered cancer-specific energy metabolism in Rh30 cell lines. Comparison of intermediate metabolites at 24 h after drug administration (DMSO vs. MCDi 10 μM); (a) acetyl-CoA and malonyl-CoA, (b) lactate, pyruvate, and the ratio of

lactate/pyruvate, (c) glucose-6-phosphate (G6P), 6-phosphogluconate (6-PG), ribose-5-phosphate (R5P), the ratio of G6P/R5P, and NADPH/NADP, (d) citrate, 2-oxoglutarate, succinate, fumarate and malate, (e) glutamine (Gln), and glutamate (Glu), (f) ATP and AMP. g; Suppression of lipid metabolism led to the inhibition of pyruvate influx into mitochondrial TCA cycle and inactivation of the PPP. (g) Comparison of mRNA expression levels of LDH-A, PDHK4, and G6PD in 4 cell lines of RMS at 12 h after drug intervention. All results are shown as mean ± SD of three or four independent experiments. (*, P < 0.05 vs. control; #, P < 0.01 vs. control.)

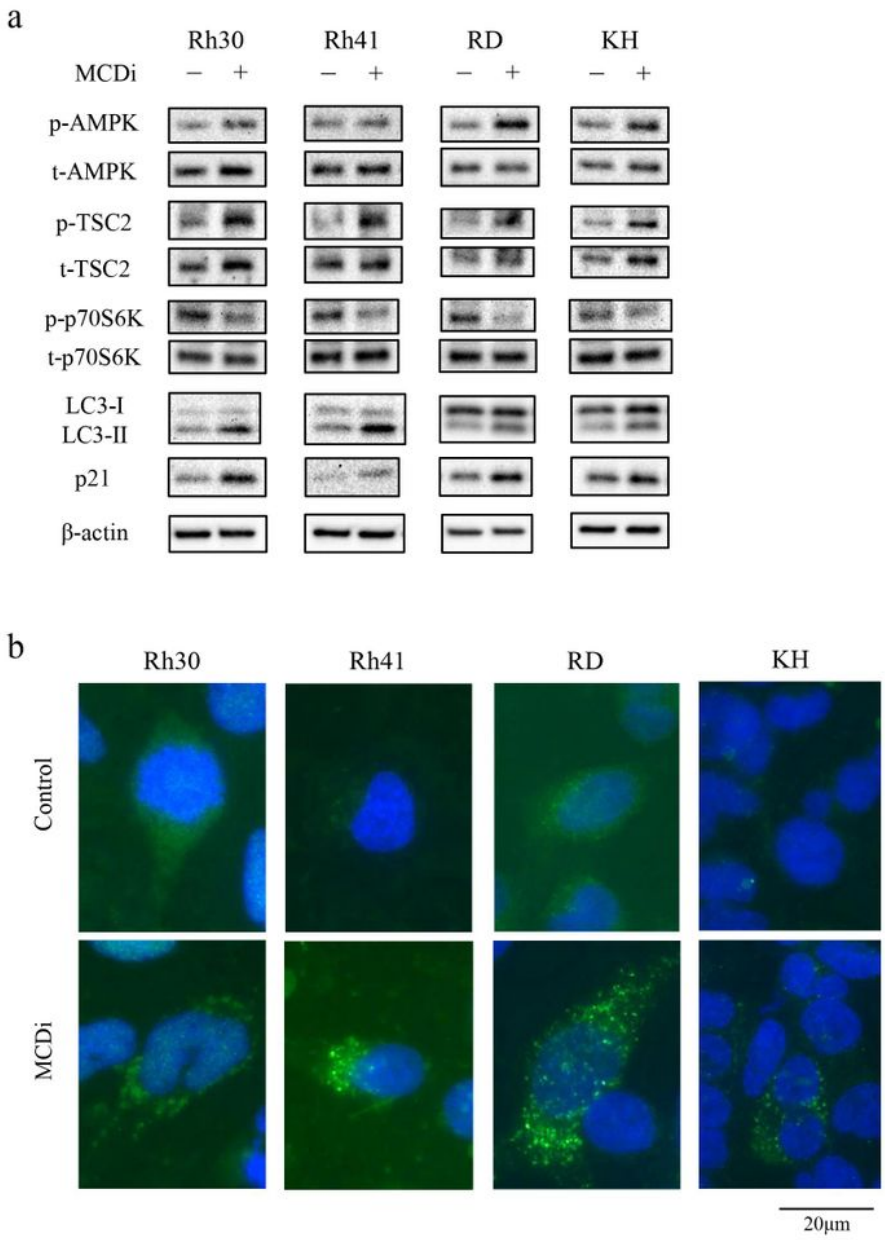

Figure 3. Miyagaki S, *et al.*

Figure 3

The inhibition of lipid metabolism induced autophagy signals through increased phosphorylation of AMPK, and increased p21 protein expression. (a) Protein expression analyses of RMS cells were performed using the samples at 24 h after the administration of DMSO or MCDi (10 μM). β actin was used as the internal control. (b) RMS cell lines were treated with DMSO or MCDi (10 μM, 48 h), followed by immunofluorescence staining with anti-LC3A/B antibody. The green spots represented the autophagosome formation, or so-called LC3 puncta. DAPI was used as a nuclear stain.

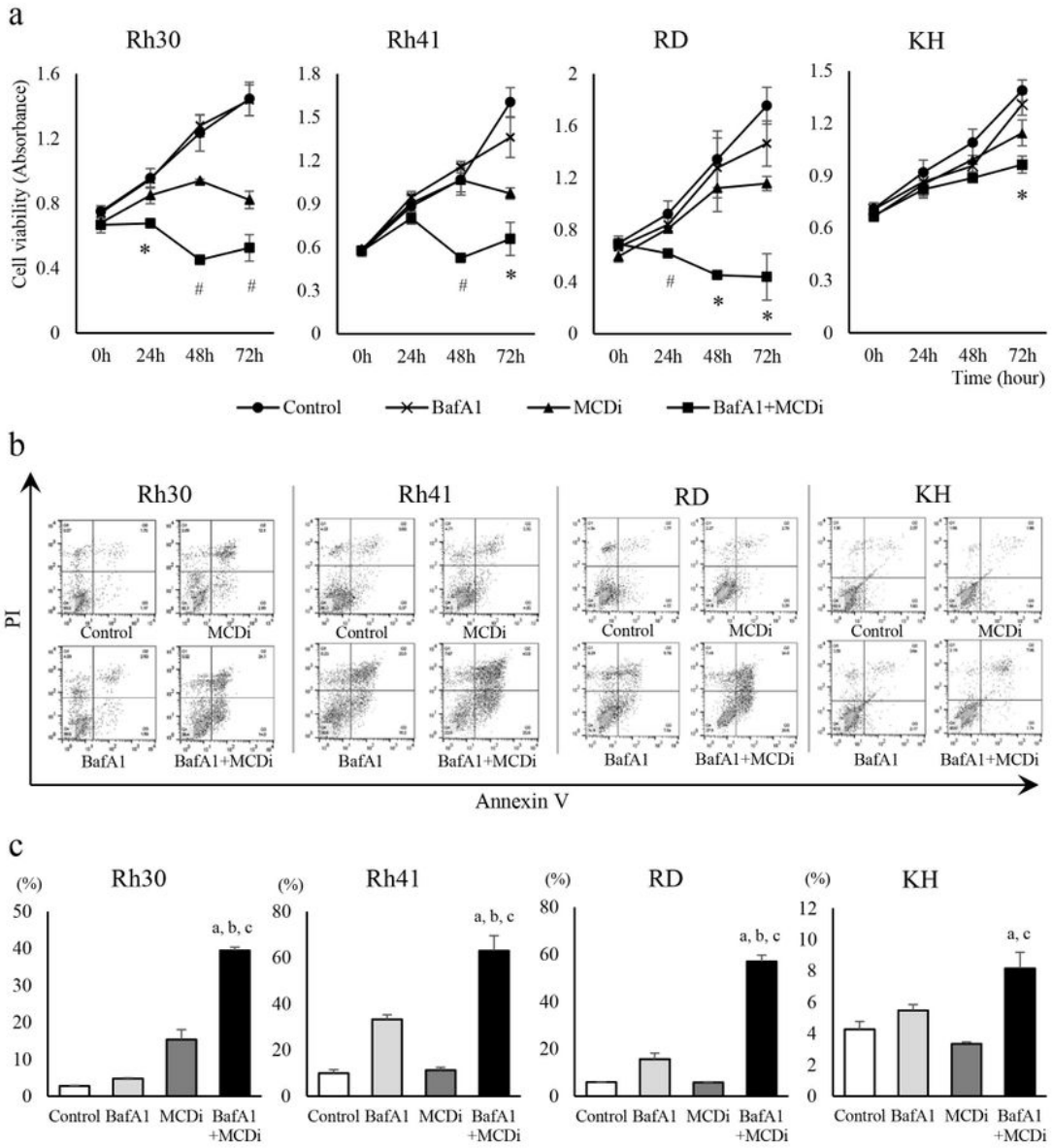

Figure 4. Miyagaki S, *et al.*

Figure 4

The inhibition of both lipid metabolism and autophagy suppressed the growth of RMS cell lines through increased apoptosis. (a) Cell viability was assessed using WST8 assay. RMS cell lines were treated with DMSO, BafA1 (2.5 nM), and/or MCDi (10 μM) for 72 h. Data are shown as mean ± SD of three or four independent experiments. (*, $P < 0.05$ vs. control; #, $P < 0.01$ vs. control.) (b) Apoptosis assay was performed. RMS cells were administered with DMSO, BafA1 (2.5 nM), and/or MCDi (10μM) for 48 h. Dot plots showed the distribution of cell populations. (c) The proportion of apoptotic cells was assessed by Annexin V-FITC and propidium iodide (PI) staining. The results are shown as mean ± SD of three independent experiments. (a, $P < 0.05$ vs. control; b, $P < 0.05$ vs. BafA1; c, $P < 0.05$ vs. MCDi.)

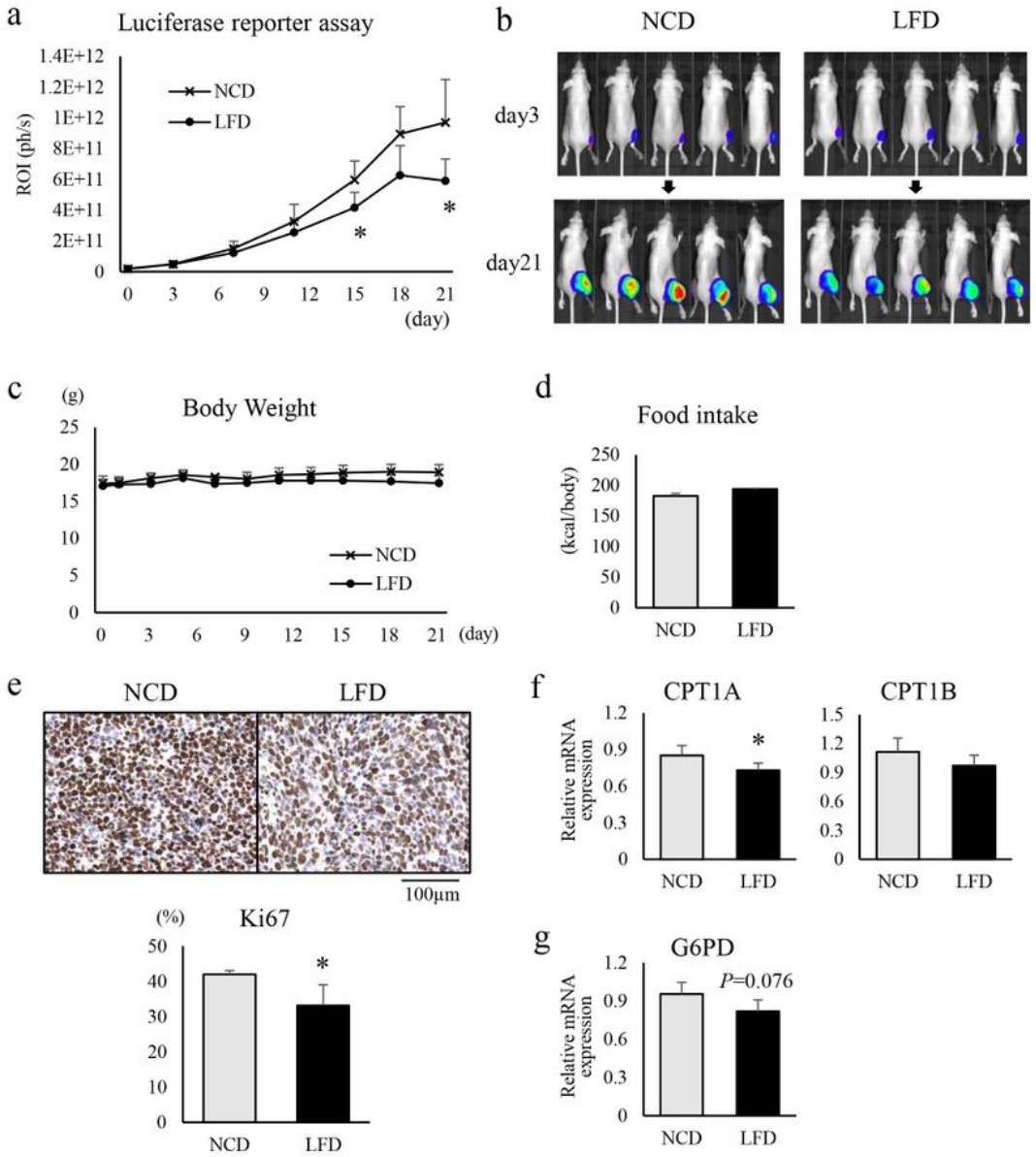

Figure 5. Miyagaki S, *et al.*

Figure 5

In an orthotopic xenograft model, LFD showed growth inhibitory effect against RMS through reduced lipid metabolism. (a) The 10 mice transplanted with luciferase-positive Rh30 cells were divided into 2 groups (5 mice each) after confirming tumor engraftment. After starting NCD or LFD, tumor growth was quantified using bioluminescence imaging. (b) Comparison of bioluminescence images on day 3 and 21 after the start of the diets. (c) Changes in body weight of the mice during the observation period. (d) The

caloric intakes of mice in the two groups were compared. (e) Tissue sections of tumor samples prepared by sacrificing mice on day 21 were immunohistochemically stained with anti-Ki67 antibody. On the upper side, representatives of the stained images of both groups are shown. A graph of Ki67 positive rate is presented below. (f, g) The CPT1 isozymes and G6PD mRNA expression levels in tumor samples from each group on day 14. All results are shown as mean ± SD, n=5 for each group. (*, $p < 0.05$ vs. NCD-fed group.)

Supplementary Files

This is a list of supplementary files associated with this preprint. Click to download.

- SupplementaryFigures.pdf
- SupplementaryTable.docx